Submitted to small NANO MICRO

DOI: 10.1002/smll.((smll.201100366)))

Nanopatterning of Ferritin Molecules and the Controlled Size Reduction of Their Magnetic Cores**

*Ramsés V. Martinez, Marco Chiesa, and Ricardo Garcia**

[*] Prof. R. Garcia, Dr. R. V. Martinez, Dr. M. Chiesa
IMM-Instituto de Microelectrónica de Madrid (CNM-CSIC)
Isaac Newton 8, PTM, E-28760 Tres Cantos, Madrid (Spain)
E-mail: ricardo.garcia@imm.cnm.csic.es
Dr. R. V. Martinez
Present address: Department of Chemistry and Chemical Biology, Harvard University
12 Oxford Street, Cambridge, MA 02138 (USA)

Supporting Information is available on the WWW under http://www.small-journal.com or from the author.

Keywords: Microcontact printing, Ferritin, Nanopatterning, Lithographically controlled wetting, Magnetic Force Microscopy

We report a nanopatterning method to deposit ferritin proteins with nanoscale accuracy over large areas. The selective deposition is driven by the electrostatic interactions existing between the proteins and nanoscale features. Upon deposition the protein shell can be removed by heating the patterns in an oxygen atmosphere. This leaves exposed the iron oxide core which can be further reduced in size by plasma etching methods. In this way, the initial ferritin molecules which have a nominal size of 12 nm are reduced to 2 nm nanoparticles. Magnetic force measurements confirm the magnetic activity of the deposited and the size-reduced nanoparticles.

1. Introduction

Micro and nanopatterning is central to modern science and technology. The advancement of microelectronics in terms of cost and performance is intrinsically linked to the development of novel lithographic methods. The need to incorporate organic and biological molecules as active parts of micro or nanoelectronic circuits is motivating the research on alternative or non-conventional patterning techniques based on soft lithography.[1-4]

Microcontact printing (μCP) has gained considerable attention in recent years as a novel and inexpensive patterning approach at the micro and nanoscales.[2] During the printing process, organic or inorganic molecules are transferred from a stamp to a rigid or flexible substrate. The molecules adsorb on the substrate surface forming a self-assembled monolayer (SAM) which chemically modifies the surface. Subsequently, the printed monolayer can be used as an etch resist. To date, gold,[5-6] silver,[7] copper,[8] silicon,[9-10] silicon dioxide,[11] and glass[12] have been patterned by using different SAMs as etch resists. Furthermore, printed SAMs can be used as a template to control selective growth of organic and inorganic materials on different substrates[13] or to guide site-selective wetting or electropolymerization. Microcontact printing facilitates patterning of materials on large-area and/or curved substrates without using standard optical lithography. Therefore, microcontact printing has become a widely used technique in organic and/or large-area electronics, biochemistry, and material science.

The use of microcontact printing in combination with selective dewetting is a generic approach that facilitates the patterning of conducting and semiconducting polymers, and resists.[14] For example, conducting and semiconducting polymers were patterned to realize organic thin-film transistors.[15] Furthermore, selective wetting was used to pattern prepolymers. Subsequently, the prepolymers were used as an etch mask to pattern silicon substrates by wet-chemical etching.[16] More recently, the technique has been applied to pattern biomolecules such as proteins or DNA with nanoscale accuracy. Lithography controlled wetting has shown its ability to pattern soluble functional materials[4,17] with sub-500 nm accuracy. Parallel methods based on the spatial confinement of electrochemical

reactions have been applied to pattern a variety of self-assembled monolayers[18] or to form polymeric structures with submicrometer periodicities.[19-20]

Nanoparticles have recently attracted great interest because of their potential to be used as components in nanotechnology. In particular, the use of metal nanoparticles is a very exciting research field because they can be used for various applications such as nanoelectronic devices, optics and sensors.[21-23] Metallic nanoparticles have often been used as seed for the growth of other useful nanostructures, such us silicon nanowires or carbon nanotubes, using chemical vapor deposition processes.[24-25] Since the diameter and the position of grown nanostructures depend on the size and location of the seed, it is desirable to synthesize metal nanoparticles with a narrow size distribution,[26] and a predefined location.[27] Micropatterning of regular arrays of iron oxide nanoparticles has been demonstrated by using a diblock copolymer micelles approach.[28]

A very appealing system is represented by ferritin, a protein whose function in living cells is the storage and controlled release of iron.[29] Ferritin is composed of 24 proteic sub-units forming a 12 nm hollow shell, called apoferritin, surrounding an iron-based core with a diameter of approximately 7 nm, whose structure resembles that of ferrihydrite $(FeOOH)_8(FeOH_2PO_4)$. The structure of apoferritin, presenting channels between the proteic sub-units, used by living cells to transfer the iron ions from and to the blood, has made possible its use as a nanoreactor for the synthesis of inorganic nanoparticles of different composition.[30-31] Importantly, it is possible to control the composition of the core without affecting the properties of the polypeptide shell. For this reason, it is possible to use the same nanopatterning process for a variety of nanoparticles.

In order to transfer the ordering of the ferritin array to a pattern of the nanoparticle, one needs to eliminate the proteic shell without losing the mineral core. Exploiting the fact that the thermal stability of proteins is lower than that of the mineral core, many authors have

proposed controlled pyrolysis at temperatures higher than 400 ºC as a method to obtain nanoparticles from ferritin. The method has been used to obtain nanoparticles both in volume and in ordered arrays deposited on surfaces. Iron nanoparticles encapsulated by graphitic shells were synthesized by ferritin pyrolysis in vacuum at 900 ºC.[32] The pyrolysis has been performed in inert[33] or oxidizing atmosphere.[34] In either case, it is possible to subsequently reduce the oxide to obtain iron nanoparticles. The size of the nanoparticles can be controlled by reaction with a chelating agent such as nitrilotriacetic acid.[35]

In this paper, we demonstrate a method that enables large scale patterning of biomolecular carriers with sub-100 nm accuracy. We also show the iron oxide core of the nanoparticles can be further reduced in size by a plasma etching treatment. Magnetic force microscopy measurements show the magnetic activity of both the as-deposited and the size-reduced nanoparticles.

2. Results and Discussion

2.1. Controlled ferritin nanopatterning at cm^2 scale

Figure 1 schematizes the process to form parallel arrays of ferritin lines covering cm^2 regions. During the initial printing process the polydimethylsiloxane (PDMS) stamp is brought in conformal contact with the substrate, so that the octadecyltrichlorosilane (OTS) molecules are transferred from the stamp to the substrate in the regions of contact. OTS consists of an alkyl ($C_{18}H_{37}$) group and a polar ($SiCl_3$) head group. The OTS head bonds to the surface by forming Si–O–Si bonds on the −OH terminated substrate. As a result the regions covered by OTS become hydrophobic, whereas the unexposed regions remain hydrophilic (see Figure 1c). The surface wetting behavior of the two regions was characterized by water contact angle measurements. Contact angle measurements have been performed on silicon surfaces entirely

functionalized with APTES and OTS using microcontact printing to verify the good quality of the monolayers in good agreement with measurements in the literature.[36-37]

Once the Si surface has been functionalized with OTS, the sample is dip coated with 3-aminopropyltriethoxysilane (APTES). APTES forms an amino-terminated monolayer ($-NH_2$) in the hydrophilic region of the substrate, while it does not grow over the hydrophobic regions (see Figure 1d). Depending on the pressure exerted during the microcontact printing of the OTS monolayer the shape of the meniscus created between stamp and sample can be modified (see Figure 1b). This control of the printing allows duplicating the number of features replicated over the silicon substrate. The resolution of the selective deposition depends on the width of the proteinphylic domains that is determined by both the stamp and the pressure exerted. The selective deposition of ferritin molecules at pH 6.5 is possible over these substrates as depicted in Figure 1f. Ferritin nanostructures down to 100 nm can be patterned by using this method.

Biological amphoteric molecules such as proteins contain both acidic and basic functional groups which derived from amino acid side chains. The isoelectric point (pI) of horse spleen ferritin is in the 4.1–5.1 range.[38] This indicates that the charge of whole ferritin molecules can be easily controlled by varying the pH of the ferritin solution. Therefore, it is expected that the ferritin molecules can be immobilized onto either cationic or anionic surfaces by changing the electrostatic interaction between the ferritin molecule and the precursor film.[39]

Figure 2 shows the accuracy of the ferritin nanopatterning at pH 6.5 over amino-terminated domains. The surface coverage that can be observed in Figure 2d is ca. 3300 particles μm^{-2}. Remarkably, there are no ferritin features outside the patterned area. This observation was reproduced in other regions millimeters away from the area shown in Figure 2d. We attribute the origin of the preferential interactions between the ferritin molecules and APTES functionalized domains to the attractive electrostatic interaction between the amino-

terminated surface and the negative charges on the ferritin at pH 6.5 (>pI).[40] The high preferentiality of this method is also enhanced by the proteinphobic behavior of the OTS domains which allows the cleaning of the ferritin molecules deposited over them when the sample is rinsed after ferritin deposition.

The polydimethylsiloxane (PDMS) stamps used in these experiments were fabricated by replicating the features of a non-recorded digital versatile disc (DVD).[41] These stamps limit the resolution of this technique to their pitch: 720 nm (see Figure 2b). To overcome this limitation on the pattern periodicity and allow the fabrication of sub-100 nm ferritin structures without requiring PDMS stamps fabricated with sub-100 nm features, we propose to control the pressure exerted by the stamp during the silicon substrate functionalization.

Figure 3 shows the formation of 90 nm wide ferritin structures by controlling the applied pressure between the stamp and the substrate, during the OTS functionalization. This is achieved by using a micrometric screw. Immediately after the natural conformation of the PDMS stamp (soaked with OTS) and the silicon surface both were separated by about 3 µm. This separation splits the OTS solution menisci generated at the first contact. A scheme of the OTS solution menisci before and after the separation can be seen in Figure 1b (top and bottom, respectively). This simple trick duplicates the number of ferritin patterns fabricated by each single protrusion in the stamp. The AFM phase image shown in Figure 3d shows the accuracy and preferentiality of the patterning method.

The patterning approach described here is limited by the selective-wetting process, rather than the microcontact printing process. It is possible to achieve sub-100 nm structures by microcontact printing.[14] Nevertheless, the fabrication process and resolution of the patterned features are influenced by the printing of the SAM, which is again influenced by the master and PDMS stamp. The aspect ratio of the PDMS stamp strongly influences the printed features. Using an epoxy resist to prepare the master results in high aspect ratios of 5–15

because the epoxy film is typically relatively thick (10–30 nm). Such high aspect ratios are of particular interest if the packing density of the printed structures is relatively low. Otherwise, sagging of the PDMS stamp occurs, which distorts the printed features.[42] To achieve the minimum possible feature size, the aspect ratio must be reduced. Reducing the aspect ratio of the relief structures and redesigning the device geometries can minimize the problem.

2.2. Magnetic force microscopy characterization of the magnetic nanoparticles enclosed in the biomolecular carriers

The ferritin carries a magnetic nanoparticle with a dipole moment of ~345 Bohr magnetons (μ_B=9.274 x10^{-24} J T^{-1}).[43] To demonstrate that the magnetic properties of the encapsulated iron-core nanoparticle are preserved by the patterning process, magnetic force microscopy (MFM) experiments have been performed on the ferritin patterned surfaces. To minimize sensitivity problems[44-46] due to the small magnetic moment of a single ferritin molecule at *T*=295 K, the experiments have been performed on protein patterns where the proteins are grouped into clusters or agglomerates of several ferritin molecules (**Figure 4**a). The magnetic moments of the ferritin cores were aligned by applying a magnetic field of 0.22 T perpendicular to the sample surface. A magnetic force microscopy (MFM) phase image of the region shown in Figure 4a was taken in the lift mode with the magnetic probe placed 20 nm above the surface (Figure 4b). The magnetic nature of the ferritin nanoparticles is demonstrated by the fact that the regions covered by ferritin appear dark with respect to the uncovered regions. We observe that the magnetic-induced phase shift varies from nanoparticle to nanoparticle. In the MFM image we identify three major classes (circles in Figure 4b). Their topography features are also circled (Figure 4a). By comparing the magnetic contrast and the topography we deduce that the magnetic contrast is associated with the

cluster size. The particles that show the strongest magnetic contrast are also larger. The magnetic phase shift signal of the circled areas changes by a factor 4 from particle 1 to 3. Several experiments have been performed to rule out the presence of topography and electrostatic interactions in the observed contrast (Figure S1, Supporting Information). In particular, it has been shown that the magnetic contrast is inverted by inverting the magnetic polarity of the magnetic probe (Figure S1).

2.3. Size reduction of magnetic nanoparticles

The patterning method described above is compatible with different processing protocols. This is illustrated by reducing the nanoparticle size and density upon deposition. The apoferritin shell is removed to generate a nanopattern formed exclusively by iron-based nanoparticles. The protein shell is removed by heating the sample up to 500 ºC in an O_2 atmosphere.[34] **Figures 5**a and 5b show a section of the pattern before heating and Figures 5d and 5e show the result obtained after the pattern has been heated at 500 ºC for 10 minutes. The comparison between the AFM phase images taken before and after heating reveals the disappearance of the protein shell (Figures 5b and 5e). The lighter halo observed in Figure 5b (see also Figure 2e) has disappeared in Figure 5e. This indicates that the apoferritin shell has been consumed in the oxygen atmosphere. The particles left correspond to the iron cores. The process also removes approximately 1/3 of the iron clusters. Contact angle measurements (Figure S3, Supporting Information) indicate that the pyrolysis destroys the self-assembled monolayers of OTS and APTES.

After the removal of the protein shells, the metallic oxide clusters can be further reduced in size by exposing them to plasma etching in an oxygen atmosphere (Figure 5g). The particle height decreases rather linearly with the plasma etching time. This process might oxidize and

vaporize the outer iron atoms. However, it does not change the particle density (inset). The whole process leads to the formation of patterns made by iron oxide particles of up to about 2 nm in size. Figures 5c and 5f show the histograms of the nanoparticle height before (Fig. 5c) and after pyrolysis and plasma etching for 120 s (Fig. 5f). Before the pyrolysis the mean height of the particles is about 8 nm which is the typical value measured by AFM.[47] Once the pattern is exposed to plasma etching for 120 s the mean height is reduced to 2 nm. It is known that the composition of the iron nanoparticles obtained upon different treatments can vary in nature.[34,48] In any case, MFM experiments (Figures S4 and S5) show that the magnetic moment of the nanoparticles has not been destroyed by the pyrolysis and O_2 plasma processes. The exact nature and composition of the resulting particles is currently under investigation.

3. Conclusions

Here we have combined several soft lithography schemes, namely microcontact printing and lithographically controlled wetting, together with bottom-up electrostatic interactions to pattern surfaces with arrays of ferritin molecules. By using magnetic force microscopy we show that the patterning process does not alter the magnetic properties of the iron oxide core. We also develop a process that enables the reduction of the nanoparticles size by exposing them to plasma etching. Thus, patterning of 2 nm particles is achieved.

4. Experimental Section

Substrate preparation and stamp fabrication: Silicon wafers (p-type) with a resistivity ρ = 10-20 Ω cm have been used as substrates for the selective deposition of biomolecular carriers. The silicon surface was cleaned by sonicating it three times in a bath of $NH_4OH/H_2O_2/H_2O$ (1:1:2) for 12 min each. This process ensures an optimum distribution of hydroxyl groups (−OH) over the surface. After the cleaning procedure the samples were immersed in a solution

of $NH_4OH/H_2O_2/H_2O$ (1:1:4) at 80 ˚C for 30 min in order to reduce its roughness and increase the number of hydroxyl groups over the surface.[49] Finally, the samples were rinsed by sonication in deionized water (5 min) and blown dry in N_2.

To fabricate the stamps for the microcontact printing, the polydimethylsiloxane (PDMS) prepolymer and the curing agent (Sylgard 184, Dow Corning, Midland) were mixed in a 10:1 curing ratio and poured onto a plastic master. The uncured PDMS was then spread by tilting the master and degassed in a vacuum chamber. PDMS stamp were cured at 80 ˚C for 4 hours.

OTS microcontact printing: Octadecyltrichlorosilane (OTS) at 90% was acquired from Sigma Aldrich and used as received. To prepare 1 mM solution, 25 μL of the starting solution were mixed with 10 mL of anhydrous toluene.

To fabricate the OTS monolayer over silicon surfaces via microcontact printing a PDMS stamp was lightly pressed against a tissue paper soaked with the OTS solution. The inked stamp was then gently pressed against a fresh prepared silicon surface for 1 minute at a controlled pressure. The formation of a nanoscale liquid meniscus between each protrusion of the soft stamp and the silicon surface enabled the transfer of the molecules from the stamp to the sample functionalizing that area. The lateral size of the meniscus determines the number of molecules deposited per unit of pattern width. The meniscus size is controlled by the applied load. The OTS-functionalized silicon surface was successively sonicated for 10 min in toluene, chloroform, ethanol, and water. Finally, the surface was blown dry in N_2.

APTES functionalization: To prepare APTES monolayers, the silicon wafer was immersed for 40 min at room temperature in a 1 mM solution of APTES in absolute ethanol. Then, it was rinsed with ethanol and dried under nitrogen. APTES was purchased form Sigma-Aldrich and used as received. Silicon surfaces functionalized with APTES/OTS nanopatterns were stable under room temperature and ambient pressure.

Selective biomolecular carrier deposition: Horse spleen ferritin (Type I) was acquired from Fluka Biochemika (Germany). The initial concentration was 85 mg mL^{-1} in a 0.15 M NaCl solution. Here, the initial concentration was diluted in deionized water by mixing 5.8 μL of the initial solution in 20 mL of water. The solution containing the proteins had pH 6.5 and was deposited on the silicon surfaces for 30 s, the sample was then rinsed in deionized water, and blown dry in N_2.

AFM and MFM analysis of the ferritin magnetic cores: The samples were imaged in air using Multimode AFM with the Nanoscope 3a controller equipped with the Quadrex Extender (Veeco Instruments, Santa Barbara, CA). For amplitude modulation AFM imaging we have used doped n^+-type silicon cantilevers (Nanosensors, Germany). The force constant k and resonant frequency f_0 were about 42 N m^{-1} and 320 kHz, respectively. The cantilever was excited at its resonant frequency. Height, amplitude, and phase images were recorded with 512x512 data points. The fast scan rate was in the 0.8-2 Hz range. MFM experiments were recorded by interleaving the topographic (main) scan with the "lift mode" scan in which the AFM tip was made to scan the sample at a lift height comprised between 10 nm and 80 nm. AFM height images were recorded using the topographic scan lines, while the amplitude and phase images were recorded using the lift-mode scan lines. For MFM imaging, magnetically coated AFM tips (NSC18 from Mikromasch, Estonia) were used. The magnetic coating consists of ~60 nm of Co/Cr alloy with a cantilever length of 230 μm and a resonant frequency of ~75 kHz. To achieve a predominant orientation of the magnetic field along the major tip axis, the tip was magnetized prior to taking measurements by subjecting them to the field of a permanent magnet of strength 0.4 T for 5 minutes.

Pyrolysis and core size reduction: To eliminate the ferritin's proteic shell the silicon samples with ferritin arrays were exposed to a pyrolysis treatment. The pyrolysis consisted of heating the samples at 500 °C for 10 minutes in an oxygen atmosphere in an electronic oven.

Further reduction of the iron oxide core was achieved by exposing the ferritin arrays to further plasma etchings. A Reactive Ion Etcher (PlasmaLab 80, Oxford Instruments) operated at 200 W was used to plasma etch the nanoparticles in an oxygen plasma for times ranging between 10 s and 2 min.

Acknowledgements
We are thankful to Dr. J. Martinez for sharing knowledge about plasma etching. We acknowledge the financial support from the Ministerio de Ciencia, Investigación e Innovación (MAT2009-08650).

References

_[1] D. Qin, Y. Xia, G. M. Whitesides, *Nat. Protoc.* **2010**, *5*, 491.

_[2] A. Perl, D. N. Reinhoudt, J. Huskens, *Adv. Mater.* **2009**, *21*, 2257.

_[3] M. Cavallini, C. Albonetti, F. Biscarini, *Adv. Mater.* **2009**, *21*, 1043.

_[4] H. M. Saavedra, T. J. Mullen, P. Zhang, D. C. Dewey, S. A. Claridge, P. S. Weiss, *Rep. Prog. Phys.* **2010**, *73*, 036501.

_[5] A. Kumar, G. M. Whitesides, *Appl. Phys. Lett.* **1993**, *63*, 2002.

_[6] T.-C. Lee, P.-C. Chen, T.-Y. Lai, W. Tuntiwechapikul, J.-H. Kim, T. R. Lee, *Appl. Surf. Sci.* **2008**, *254*, 7064.

_[7] Y. Xia, N. Venkateswaran, D. Qin, J. Tien, G. M. Whitesides, *Langmuir* **1998**, *14*, 363.

_[8] Y. Xia, E. Kim, M. Mrksich, G. M. Whitesides, *Chem. Mater.* **1996**, *8*, 601.

_[9] K. R. Finnie, R. Haasch, R. G. Nuzzo, *Langmuir* **2000**, *16*, 6968.

_[10] H.-W. Li, B. V. O. Muir, G. Fichet, W. T. S. Huck, *Langmuir* **2003**, *19*, 1963.

_[11] G. Tizazu, A. M. Adawi, G. J. Leggett, D. G. Lidzey, *Langmuir* **2009**, *25*, 10746.

_[12] S. Y. Ku, K. T. Wong, A. J. Bard, *J. Am. Chem. Soc.* **2008**, *130*, 2392.

_[13] Z. Huang, P.-C. Wang, A. G. MacDiarmid, Y. Xia, G. Whitesides, *Langmuir* **1997**, *13*, 6480.

_[14] F. S. Marikkar, C. Carter, K. Kieltyka, J. W. F. Robertson, C. Williamson, A. Simmonds, R. Zangmeister, T. Fritz, N. R. Armstrong, *Langmuir* **2007**, *23*, 10395.

_[15] A. Benor, B. Gburek, V. Wagner, D. Knipp, *Org. Electron.* **2010**, *11*, 831.

_[16] S. A. Ruiz, C. S. Chen, *Soft Matter* **2007**, *3*, 168.

_[17] M. Cavallini, F. Biscarini, *Nano Lett.* **2003**, *3*, 1269.

_[18] A. Zeira, D. Chowdhury, R. Maoz, J. Sagiv, *ACS Nano* **2008**, *2*, 2554.

_[19] R. V. Martinez, N. S. Losilla, J. Martinez, Y. Huttel, R. Garcia, *Nano Lett.* **2007**, *7*, 1846.

_[20] R. Garcia, N. S. Losilla, J. Martinez, R. V. Martinez, F. J. Palomares, Y. Huttel, M. Calvaresi, F. Zerbetto, *Appl. Phys. Lett.* **2010**, *96*, 143110.

_[21] R. J. Tseng, J. X. Huang, J. Ouyang, R. B. Kaner, Y. Yang, *Nano Lett.* **2005**, *5*, 1077.

_[22] C. Huang, A. Bouhelier, G. C. des Francs, A. Bruyant, A. Guenot, E. Finot, J. C. Weeber, A. Dereux, *Phys. Rev. B* **2008**, *78*, 155407.

_[23] A. T. Gates, S. O. Fakayode, M. Lowry, G. M. Ganea, A. Murugeshu, J. W. Robinson, R. M. Strongin, I. M. Warner, *Langmuir* **2008**, *24*, 4107.

_[24] M. Tominaga, A. Ohira, A. Kubo, I. Taniguchi, M. Kunitake, *Chem. Commun.* **2004**, 1518.

_[25] J.-Y. Raty, F. Gygi, G. Galli, *Phys. Rev. Lett.* **2005**, *95*, 096103.

_[26] H. C. Choi, W. Kim, D. Wang, H. Dai, *J. Phys. Chem. B* **2002**, *106*, 12361.

_[27] A. Javey, H. Dai, *J. Am. Chem. Soc.* **2005**, *127*, 11942.

_[28] S.-H. Yun, B.-H. Sohn, J. C. Jung, W.-C. Zin, M. Ree, J. W. Park, *Nanotechnology* **2006**, *17*, 450.

_[29] P. M. Harrison, P. Arosio, *BBA-Bioenergetics* **1996**, *1275*, 161.

_[30] H. A. Hosein, D. R. Strongin, M. Allen, T. Douglas, *Langmuir* **2004**, *20*, 10283-10287.

_[31] M. Li, C. Viravaidya, S. Mann, *Small* **2007**, *3*, 1477.

_[32] S. C. Tsang, J. Qiu, P. J. F. Harris, Q. J. Fu, N. Zhang, *Chem. Phys. Lett.* **2000**, *322*, 553.

_[33] Z. Yuan, D. N. Petsev, B. G. Prevo, O. D. Velev, P. Atanassov, *Langmuir* **2007**, *23*, 5498.

_[34] S. Yoshii, K. Yamada, N. Matsukawa, I. Yamashita, *Jpn. J. Appl. Phys.* **2005**, *44*, 1518.

_[35] M. Tominaga, M. Matsumoto, K. Soejima, I. Taniguchi, *J. Colloid Interf. Sci.* **2006**, *299*, 761.

_[36] H. Li, J. Zhang, X. Z. Zhou, G. Lu, Z. Y. Yin, G. P. Li, T. Wu, F. Boey, S. S. Venkatraman, H. Zhang, *Langmuir* **2010**, *26*, 5603.

_[37] M. H. Jung, H. S. Choi, *Korean J. Chem. Eng.* **2009**, *26*, 1778.

_[38] A. G. Hemmersam, K. Rechendorff, F. Besenbacher, B. Kasemo, D. S. Sutherland, *J. Phys. Chem. C* **2008**, *112*, 4180.

_[39] R. V. Martinez, J. Martinez, M. Chiesa, R. Garcia, E. Coronado, E. Pinilla-Cienfuegos, S. Tatay, *Adv. Mater.* **2010**, *22*, 588.

_[40] K. Uto, K. Yamamoto, N. Kishimoto, M. Muraoka, T. Aoyagi, I. Yamashita, *J. Mater. Chem.* **2008**, *18*, 3876.

_[41] R. V. Martinez, N. S. Losilla, J. Martinez, M. Tello, R. Garcia, *Nanotechnology* **2007**, *18*, 084021.

_[42] Y. Huang, W. Zhou, K. Hsia, E. Menard, J. Park, J. Rogers, A. Alleyne, *Langmuir* **2005**, *21*, 8058.

_[43] S. A. Makhlouf, F. T. Parker, A. E. Berkowitz, *Phys. Rev. B* **1997**, *55*, R14717.

_[44] S. Schreiber, M. Savla, D. V. Pelekhov, D. F. Iscru, C. Selcu, P. C. Hammel, G. Agarwal, *Small* **2008**, *4*, 270.

_[45] A. Schwarz, R. Wiesendanger, *Nano Today* **2008**, *3*, 28.

_[46] C.-W. Hsieh, B. Zheng, S. Hsieh, *Chem. Commun.* **2010**, *46*, 1655.

_[47] C. Dietz, E. T. Herruzo, J. R. Lozano, R. Garcia, *Nanotechnology* **2011**, *22*, 125708.

_[48] J. W. Zheng, Z. H. Zhu, H. F. Chen, Z. F. Liu, *Langmuir* **2000**, *16*, 4409.

_[49] D. Chowdhury, R. Maoz, J. Sagiv, *Nano Lett.* **2007**, *7*, 1770.

Received: ((will be filled in by the editorial staff))
Revised: ((will be filled in by the editorial staff))
Published online on ((will be filled in by the editorial staff))

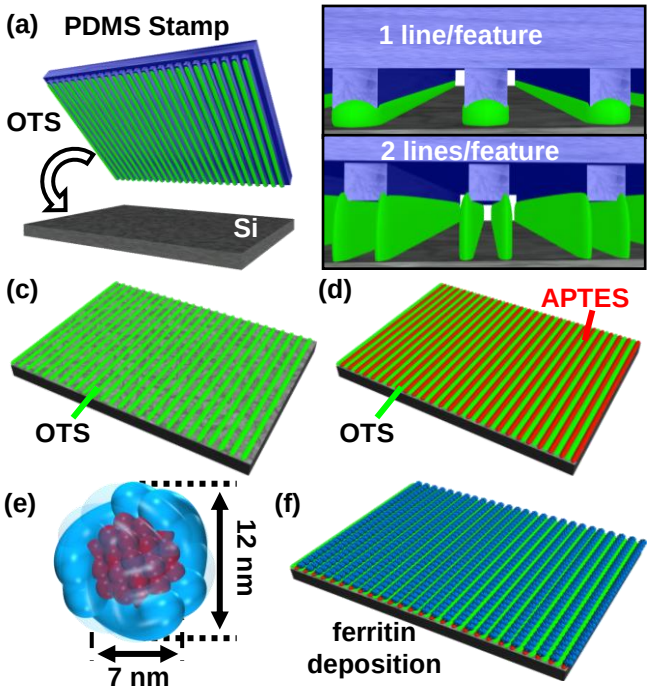

Figure 1. Scheme of the major steps required to pattern large areas of silicon surface with nanoscale features made of ferritin molecules by microcontact printing. (a) A PDMS stamp with topographical features is functionalized with OTS and put in contact with a silicon substrate. (b) Depending on the force exerted over the PDMS stamp it is possible to replicate the features with single or double accuracy. (c) OTS lines over Si substrate after microcontact printing. (d) The whole substrate shown in (c) is dipped in an APTES solution resulting in the complete coverage of the silicon substrate with hydrophilic/hydrophobic domains. (e) Ferritin molecule. (f) Ferritin controlled positioning after its deposition on (d) at pH 6.5.

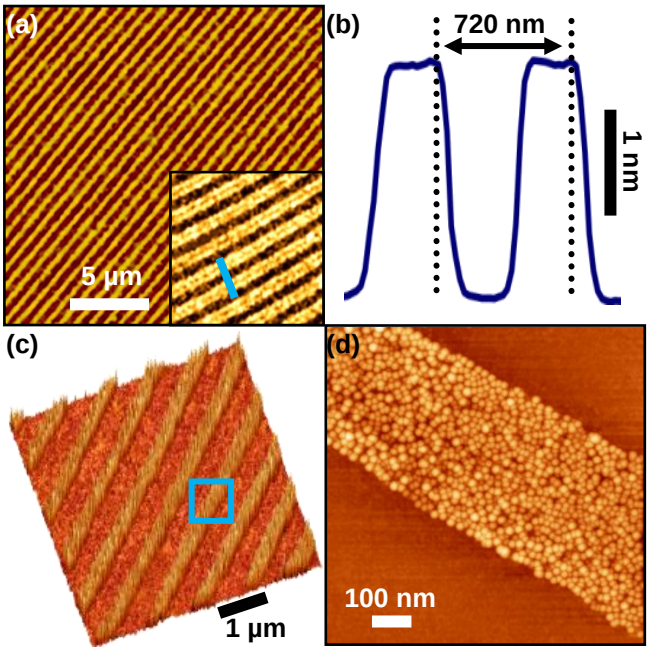

Figure 2. Preferential deposition of ferritin molecules over large-scale surfaces. (a) Amplitude modulation AFM image of the hydrophobic domains fabricated by microcontact printing. (b) AFM cross-section of the region marked in the inset of (a). The height of the pattern indicates that a complete OTS monolayer has been transferred to the silicon substrate. (c) Amplitude modulation AFM image of the preferential ferritin deposition over APTES modified silicon substrates. (d) High resolution AFM image of the region marked in (c). 100% of the ferritin molecules have been confined over the hydrophilic domains.

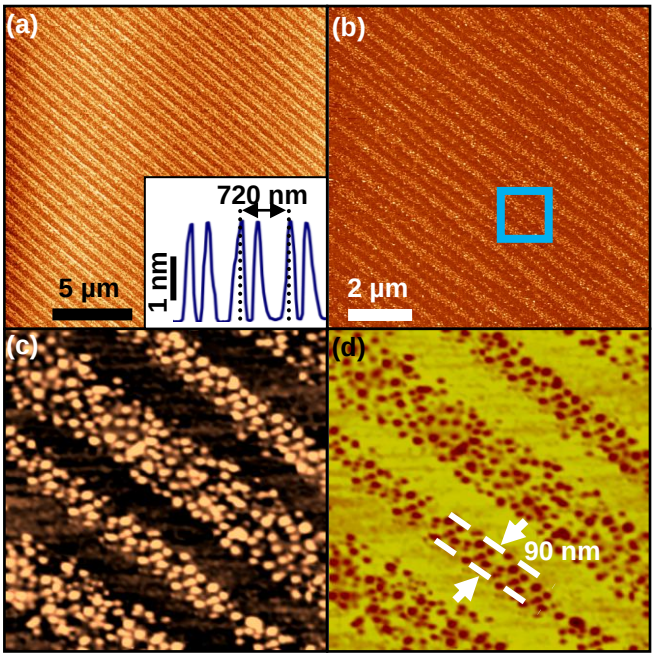

Figure 3. Preferential deposition of ferritin molecules over large-scale surfaces. (a) Amplitude modulation AFM image of the hydrophobic domains fabricated by microcontact printing. (Inset) AFM cross-section of the region marked. The height of the pattern indicates that a complete OTS monolayer has been transferred to the silicon substrate. (b) Amplitude modulation AFM image of the preferential ferritin deposition over APTES modified silicon substrates. (c) High resolution AFM image of the region marked in (b). 100% of the ferritin molecules have been confined over the hydrophilic domains. (d) Phase image of the ferritin molecules.

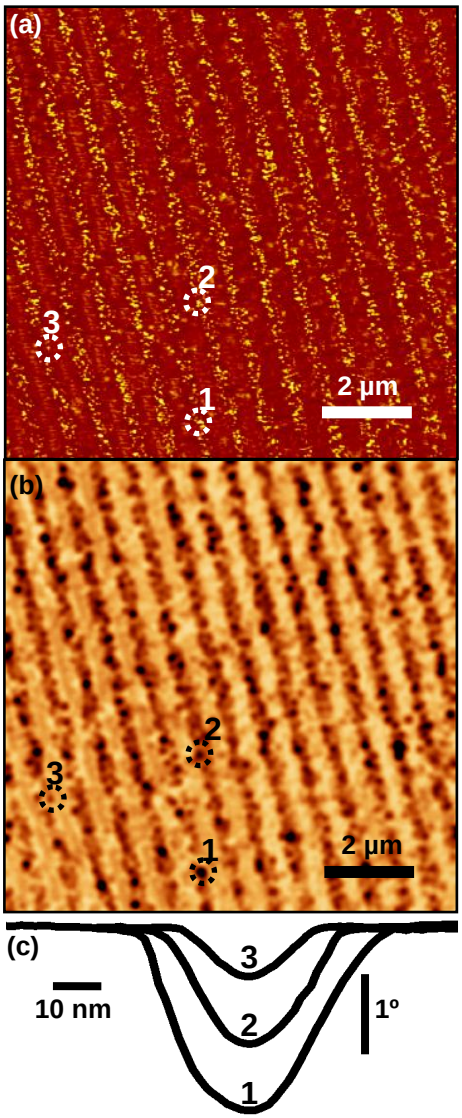

Figure 4. Magnetic force microscopy image of ferritin patterns. (a) Parallel array of ferritin lines. The line width is made of several ferritin molecules. (b) Magnetic force microscopy image of a parallel array of ferritin molecules. The magnetic contrast (dark dots) probably comes from several molecules. (c) Magnetic phase cross-sections of the particles circled in (b).

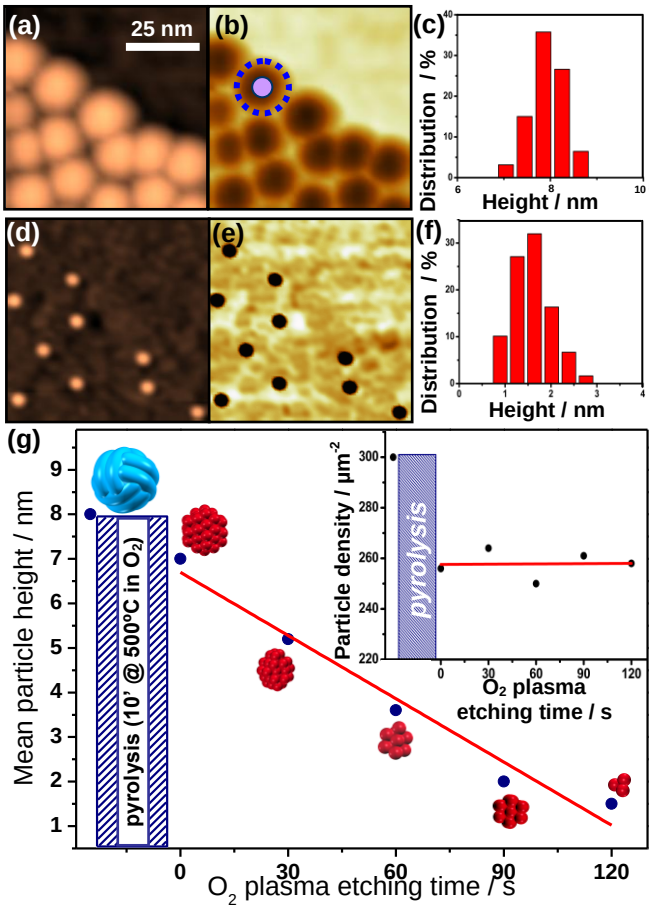

Figure 5. Evolution of the nanoparticle size and density after heating and plasma etching. (a) Topography (AFM) of a section of a pattern shown a close-packed distribution of ferritin molecules. (b) AFM phase image of the same region shown in (a). (c) Histogram of the particle height distribution before any post-deposition processing. (d) Topography (AFM) of a section of a pattern after heating the sample at 500 ˚C in O_2 for 10 minutes. (e) AFM phase image of the same region shown in (d). Note that the protein shell has disappeared. (f) Histogram of the particle height distribution after heating the sample at 500 ˚C in O_2 for 10 minutes and exposing it to plasma etching for about 2 minutes. (g) Particle size distribution as a function of the etching time. The inset shows that the particle density is not modified by the etching.

Ferritin is patterned over large areas with nanoscale accuracy by microcontact printing and controlled dewetting. Magnetic force microscopy confirms that the magnetic properties of the iron oxide cores are conserved. Pyrolysis and plasma etching enable controlled size reduction of the nanoparticles.

TOC Keyword: Ferritin, Lithographically controlled wetting, Magnetic Force Microscopy, Microcontact printing, Nanopatterning

R. V. Martinez, M. Chiesa, R. Garcia* ■<B>…<B>■

Nanopatterning of Ferritin Molecules and the Controlled Size Reduction of Their Magnetic Cores

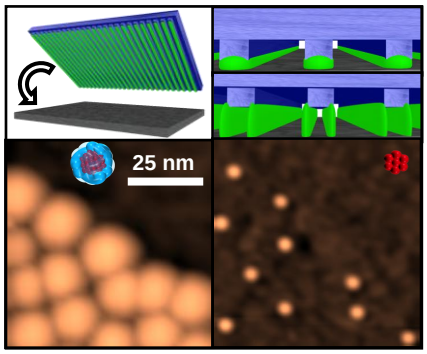

Page Headings
Left page: R. V. Martinez et al.
Right page: Patterning of ferritin and magnetic nanoparticles